

Correlation of *Fermi*–LAT sources with the AT20GHz radio survey

G. Ghirlanda^{*}, G. Ghisellini, F. Tavecchio, L. Foschini

INAF – Osservatorio Astronomico di Brera, Via Bianchi 46, I-23807 Merate, Italy

arXiv:1003.5163v1 [astro-ph.HE] 26 Mar 2010

29 March 2010

ABSTRACT

We cross correlate the *Fermi* 11 months survey catalogue (1FGL) with the 20 GHz Australia Telescope Compact Array radio survey catalogue (AT20G) composed by 5890 sources at declination $<0^\circ$. Among the 738 *Fermi* sources distributed in the southern sky we find 230 highly probable candidate counterparts in the AT20G survey. Of these, 222 are already classified as blazars (176 of known type and 46 of unknown optical class) in the *Fermi* 1-year LAT AGN Catalogue (1LAC) and 8 are new associations. By studying the γ -ray and radio properties of these associations we find a strong correlation between the γ -ray flux (above 100 MeV) and the 20 GHz flux density. This correlation is more than 3σ statistically significant both for the population of BL Lacs and of FSRQ considered separately. We also find that the radio counterparts associated to the *Fermi* sources have on average flat radio spectra between 5 and 20 GHz and that *Fermi* γ -ray sources are not preferentially associated with “ultra inverted spectrum” radio sources. For 2 of the 8 new associations we build the broad band spectral energy distribution combining *Fermi*, *Swift* and radio observations. One of these two sources is identified with the high redshift FSRQ Swift J1656.3–3302 ($z = 2.4$) and we classify the other source as a candidate new FSRQ. We also study the brightest radio source of the 46 associations without an optical classification and classify it as a new BL Lac candidate “twin” of the prototypical BL Lac OJ 287 if its redshift is somewhat larger, $z \sim 0.4$.

Key words: BL Lacertae objects: general — quasars: general — radiation mechanisms: non-thermal — gamma-rays: theory — X-rays: general — radio continuum: general

1 INTRODUCTION

The Large Area Telescope (LAT) on board the *Fermi* satellite (Atwood et al. 2009) detected 1451 sources in the γ -ray band above 100 MeV with a significance $>4.5\sigma$ during its first 11 months survey (Abdo et al. 2010, A10 hereafter). This is the 1FGL catalogue¹ and contains both galactic and extragalactic γ -ray sources. In a recent paper Abdo et al. (2010a, A10a hereafter) classified 831 out of 1451 1FGL sources as blazars. These form the 1LAC catalogue². Considering the 796 sources in the 1LAC associated with a single counterpart, there are 37 sources generically classified as AGN, 314 BL Lac and 285 Flat Spectrum Radio Quasars (FSRQ), classified according to their optical spectrum. The remaining 160 sources are candidate blazars but of “unknown” class because of lacking an optical spectrum or, if available, because of its poor quality for the optical classification. However, for these sources a counterpart could still be found in one of the radio catalogues adopted for the source identification by A10a (CRATES – Haeley et al. 2007; CGRaBS – Healey et al. 2008; the BZCat – Massaro et al. 2009). Thirty five

sources in the 1LAC sample have more than one associated counterpart.

The 1FGL sample is equally populated in the northern (713 sources) and southern sky (738 sources). However, only 50% of the 1FGL sources in the south sky are classified as blazars in the 1LAC catalogue with respect to $\sim 70\%$ of the 1FGL northern sources which are classified as blazars in the 1LAC catalogue.

The recently published Australia Telescope 20 GHz Survey (AT20G, Murphy et al. 2010) represents the largest catalogue of high frequency radio sources detected with the Australia Telescope Compact Array (ATCA) in a survey conducted from 2004 to 2008 and covering the whole sky south of declination 0° . It contains 5890 radio sources with flux at 20 GHz exceeding 40 mJy and it is complete at a level of 91% above 100 mJy beam $^{-1}$. For several sources the fluxes at 8 and 5 GHz are also measured. The AT20G survey, being conducted at relatively high radio frequencies (20 GHz), most likely detects the radio emission from the compact cores of AGN. Several sources in this survey have flat or inverted radio spectra between 5 and 20 GHz.

We correlate the AT20G radio catalogue with the 1FGL in search for possible counterparts. This allows us to study the radio versus γ -ray properties of these associations. A possible correlation between the radio and the γ -ray emission in radio loud AGN can shed light on the physical link between the emission pro-

^{*} Email: giancarlo.ghirlanda@brera.inaf.it

¹ http://fermi.gsfc.nasa.gov/ssc/data/access/lat/1yr_catalog/

² <http://heasarc.gsfc.nasa.gov/W3Browse/fermi/fermilac.html>

cesses in these two energy bands. The νF_ν spectra of both FSRQ and BL Lac objects show two peaks which are widely interpreted as due to the synchrotron and inverse Compton emission, respectively. The Spectral Energy Distribution (SED) of blazars form a sequence (so-called “blazar sequence”, e.g. Fossati et al. 1998) with the most powerful sources (FSRQs) having the synchrotron and Inverse Compton peaks in the IR and MeV energy range respectively, while the less powerful BL Lacs have the synchrotron and Inverse Compton peak in the optical/UV (or even X-ray) and GeV–TeV energy range respectively. The blazar sequence was built by dividing blazars into bins of radio luminosity, thought to be a proxy for the bolometric one, and establishes a link between the radio and the γ -ray emission.

Before *Fermi*, no conclusive claim could be made on the existence of a possible correlation between radio and γ -ray properties for EGRET sources (e.g. Mucke et al. 1997). Taylor et al. (2007), by studying the radio properties of EGRET detected blazars with the VLBA Imaging and Polarimetry Survey (VIPS – extending down to 85 mJy) found that at low radio fluxes the radio flux density does not directly correlate with the γ -ray flux. Further investigation of this correlation was possible with the source list of the *Fermi* first three months survey (LBAS, Abdo et al. 2009; Giroletti et al. 2010): while a correlation between the radio flux at 8.4 GHz and the peak flux (above 100 MeV) appears when considering BL Lacs and FSRQ together, the statistical evidence is only marginal for FSRQs (chance correlation probability of 8%), being more robust only for BL Lacs (0.5%). Such correlation analysis should consider the different redshift range spanned by these two populations (e.g. Mucke et al. 1997). Abdo et al. (2009) found a separation in the γ -ray spectral index versus radio luminosity among FSRQs, BL Lacs and misaligned AGN which suggests that more luminous radio sources have softer γ -ray spectra. Recent studies of the radio– γ flux correlation in the LBAS sources (Kovalev et al. 2009; 2009a) was conducted using the MOJAVE sample of extragalactic sources (with a flux limit of 1.5 Jy at 15 GHz). Kovalev et al. (2009) find that the parsec-scale radio emission and the γ -ray flux are strongly related in bright γ -ray objects, suggesting that *Fermi* selects the brightest objects from a flux–density limited sample of radio–loud sources.

In this paper we search for the possible counterparts of the *Fermi* 1FGL sample in the AT20G survey (§1). By intersecting the association results with the 1LAC sample we study the radio vs γ -ray properties of these associations (§2). The 1FGL–AT20G correlation also reveals 8 new associations which are unclassified sources in the 1FGL sample. For two of these there are *Swift* observations which, combined with the radio and *Fermi* data, allow to build the broad band SED. One of these two sources is classified here as a new candidate FSRQ (§3). We also present, as a first result of an on-going study of the properties of the 46 unknown sources of the 1LAC sample, the SED of the brightest radio source of the UIS class that we associate with one 1FGL source. We classify this object as a BL Lac due to the similarity of its SED to that of OJ 287 (§4). We discuss our findings in §5.

2 *Fermi*–LAT 1FGL / AT20G CROSS CORRELATION

One method used to find *Fermi* counterparts (Abdo et al. 2009, 2010, 2010a) relies on positional coincidence (Sutherland & Saunders 1992) and it is based on Bayes statistics. To each association between a *Fermi* source and a candidate counterpart it is assigned a posterior probability based on the counterparts’ space density around the *Fermi* source. Only those associations with a posterior

probability larger than a chosen value are considered as likely associations. Considering only high latitude sources ($|b| > 10^\circ$) the 1LAC sample (Abdo et al. 2010) contains 709 AGN counterparts (i.e. also multiple counterparts within the *Fermi* source error ellipse) associated to 671 *Fermi* 1FGL sources at high galactic latitudes with posterior probabilities $> 50\%$. Among these, 663 have posterior probabilities $> 80\%$ and 599 are defined as “clean” associations if (i) they have one single associations; (ii) the posterior probability is larger than 80% and (iii) are not flagged as problematic (e.g. marginal detection or data problems) in the 1FGL sample.

The method adopted by A10a to build the 1LAC sample is implemented in the `gtsrcid` tool distributed with the LAT `ScienceTools-v9r15p2` software. The association method searches for single radio sources falling within the confidence ellipse of the *Fermi* sources. We applied this method in cross correlating the AT20G survey catalogue with the 1FGL one. Similarly to the 1LAC sample we accept only single associations (i.e. only one radio counterpart falls within the the *Fermi* source error ellipse) and with a posterior probability $> 80\%$.

2.1 Prior probability of the AT20G survey

To compute the posterior probability we have to assign the prior probability to the AT20G sample. This represents the confidence that the AT20G catalogue contains the real counterparts of the *Fermi* sources. We compute the prior probability of the AT20G catalogue following the procedure described in Appendix C of A10. The prior probability represents the probability of finding a number of false identification from the correlation of the 1FGL and AT20G real catalogues which is equal to the average number of associations found by the cross correlation of the AT20G sample with randomly generated catalogues of *Fermi* sources. To this aim we created a set of 100 *Fermi* fake catalogues by displacing the sources between 2 and 10 degrees from their real positions. For sources near the galactic plane a smaller displacement in galactic latitude was adopted (Eq. C3 of Appendix C of A10).

We then computed the number of false associations between the AT20G and 1FGL as a function of the prior probability assigned to the AT20G catalogue (dashed line in Fig. 1) and the average number of associations between the AT20G and 100 1FGL random catalogues for each value of the prior probability (solid line in Fig. 1). The intersection between the two curves in Fig. 1 gives the value of the prior probability adopted for the AT20G sample.

2.2 Cross correlation results

From the cross correlation of the AT20G and the 1FGL catalogue we found 230 associations for the 738 1FGL sources distributed in the southern sky, i.e in the same sky portion covered by the AT20G survey. Among these associations 222 sources are already classified as blazars in the 1LAC sample: 10 are generically classified as AGN, 54 are BL Lac, 112 are FSRQ and 46 are of unknown type. There are 8 remaining sources which are newly found associations, i.e. they are not present in the 1LAC sample. Tab. 3 lists the properties of the 222 1FGL–AT20G associations which are classified as blazars in the 1LAC sample. In Tab. 2 we report the 8 new associations. For each association we give its posterior probability, the separation between the *Fermi* 1FGL source centroid and the position of the AT20G associated source, the 1FGL and AT20G names, the name of the AGN that was associated to the *Fermi* 1FGL source in the 1LAC sample and its optical classifica-

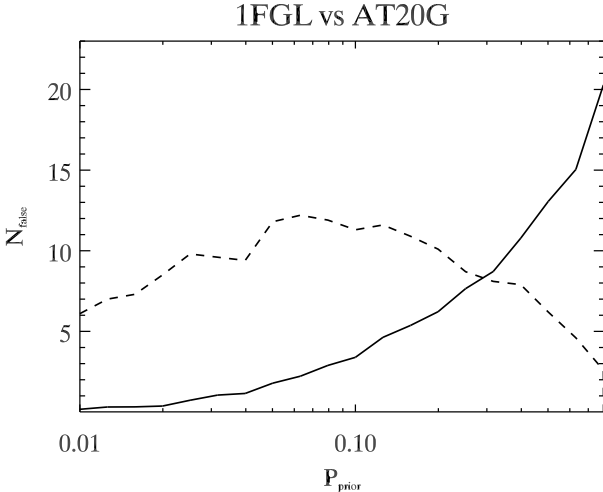


Figure 1. Number of false associations as a function of the prior probability assumed in cross correlating the AT20G survey with the *Fermi* 11 months source catalogue (1FGL) (dashed line). The solid line represents the average number of associations found by a cross correlation of the AT20G with 100 random *Fermi* catalogues (for each value of the prior probability). The intersection between the two curves represents the prior probability used in the cross correlation of the AT20G survey and the 1FGL catalogue (see A10).

tion (AGN, BLL, FSRQ or UNKNOWN) and if the 1LAC association was classified as “clean” or not. We note that in the generic class of AGN there are several types of sources: starburst galaxies (NGC 253 – Abdo et al., 2010b), starburst/Seyfert 2 (NGC 4945 – Lenc & Tingay, 2009) a Low-Excitation FRI radio galaxy (PKS 0625-35 – Gliozzi et al., 2008) a High-Excitation FRI radio galaxy (Cen A), a Narrow-Line Seyfert 1 (PKS 2004-447 – Abdo et al., 2009b). In the following plots these sources are labelled “AGN” to distinguish them from the class of BL Lacs and FSRQ. We do not enter in the details of the properties of these sub-classes of AGNs because it is out of the scope of the present paper.

Fig. 2 shows the angular separation between the 1FGL and the AT20G sources for the 230 associations found as a function of the *Fermi* detection significance (left panel) and of the posterior probability of the association (right panel). The angular separation between the 1FGL sources and the associated AT20G counterparts decreases as a function of the *Fermi* detection significance. This behaviour is common among the different blazar types. The number of associations concentrates to low significance values where also the association separation is larger. From Fig. 2 it appears also that, although our association methods selected only those with a posterior probability $> 80\%$, most of the associations found have a probability distribution (right panel of Fig. 2) that is skewed towards high probabilities ($> 95\%$) suggesting that most of *Fermi* sources with relatively low detection significance are found in associations with a high posterior probability.

3 RADIO AND GAMMA-RAY PROPERTIES OF THE AT20G-1FGL ASSOCIATIONS

In Fig. 3 we compare the distribution of the 20 GHz fluxes of all the 5890 sources of the AT20G sample with the distribution of the radio flux of those sources associated with one source of the 1FGL catalogue. The 1FGL sources select the radio counterparts with the largest fluxes within the flux-limited AT20G survey. The

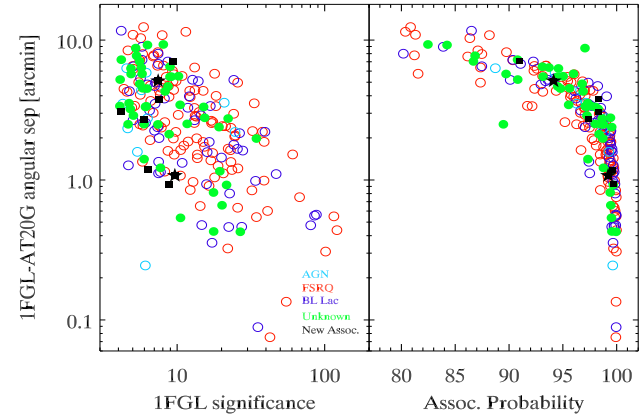


Figure 2. Angular separation between the centroid of the 1FGL source and the position of the associated AT20G source as a function of the *Fermi* detection significance (left panel) and of the probability of the association (right panel) computed with the `gt_srcid` tool. Open circles are the associations (Tab. 1) which are also present in the 1LAC sample (i.e. already identified as blazars of different types: AGN, FRSQ, BL Lac). Those which are 1LAC likely blazars but of unknown class are marked by filled (green) circles. The solid squares and stars are the new associations (Tab. 2) found from the cross correlation of AT20G and 1FGL. The star symbols are the two new associations classified as FSRQ in this paper.

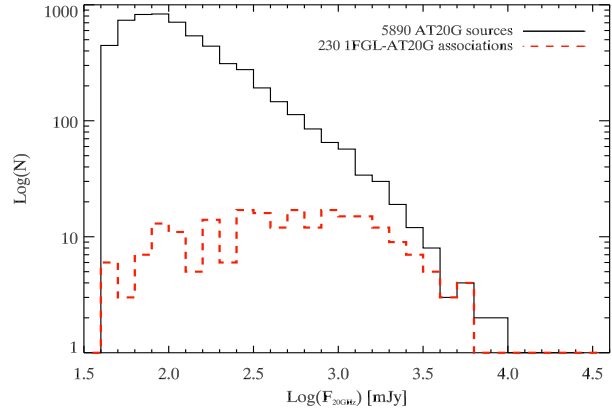


Figure 3. Distribution of the radio fluxes at 20 GHz for the 5890 sources of the AT20G sample (solid line) and of 230 sources associated with one *Fermi* 1FGL source with a probability $> 80\%$ of the association.

Kolmogorov-Smirnov (KS) test gives a probability of 1.9% that the two distributions are similar.

Selecting the associations that are blazars of known type we compare the distributions of radio fluxes of BL Lacs and FSRQs. In the LBAS sample, these were found (Abdo et al. 2009) to be different (considering the 8.4 GHz fluxes). Using our sample and the 20 GHz flux we also find that these two populations have different radio fluxes with FSRQ being on average brighter than BL Lacs (the chance probability that the two distribution are consistent being only 1.5×10^{-4}).

The radio vs γ -ray properties of the *Fermi* first 3 months catalogue (Abdo et al. 2009; Giroletti et al. 2010) showed that there is a possible correlation between the 8.4 GHz radio flux and the γ -ray flux. However, this correlation was found to be statistically significant (chance probability of 0.05%) only for the population

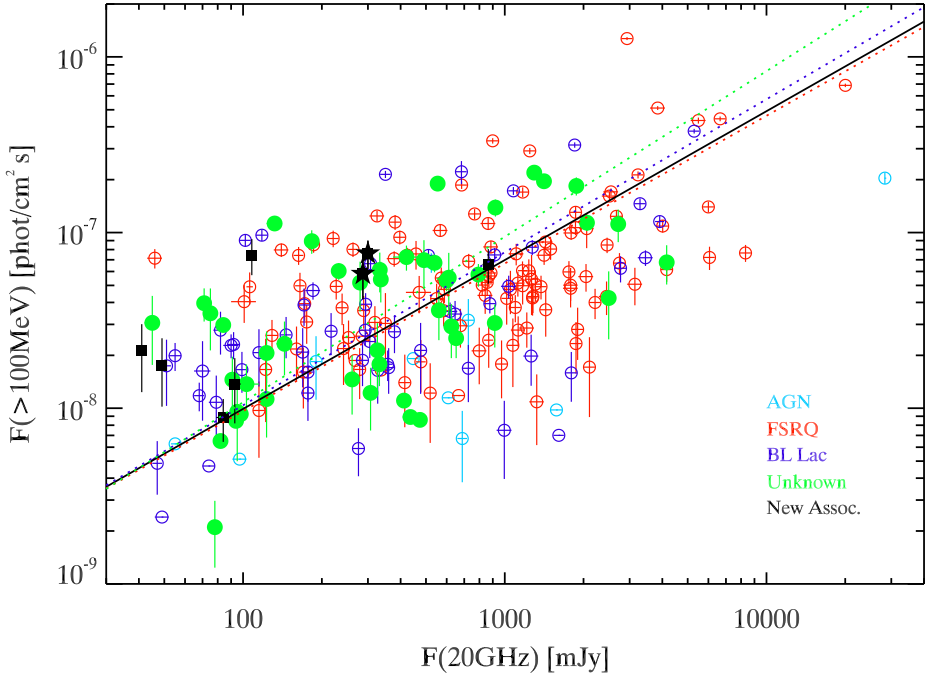


Figure 4. Correlation between the γ -ray flux (integrated above 100 MeV) and the radio flux at 20 GHz for the 230 associations found from the cross correlation of the AT20G survey and the 1FGL catalogue. Symbols are the same as in Fig. 2. The solid line is the best fit correlation of all the data points, the dotted line for FSRQ, the dashed line for BL Lac and the dot-dashed line for sources of unknown optical classification. The slopes and significance of the different correlations are reported in Tab. 1.

Sources	r_s	P	A
All (230)	0.53	10^{-17}	0.85 ± 0.04
FSRQ (112)	0.42	3×10^{-6}	0.84 ± 0.06
BL Lac (54)	0.51	9.4×10^{-6}	0.87 ± 0.07
Unknown (46)	0.58	1.9×10^{-5}	0.94 ± 0.1

Table 1. Correlation between the γ -ray flux and the 20 GHz radio flux density for all 230 associations and for different sub-samples. The Spearman correlation coefficient r_s and the chance correlation probability P are given. The correlation is fitted with a function $\log F_{>100 \text{ MeV}} \propto A \log F_{20 \text{ GHz}}$ and the slope is given in column 4.

of BL Lacs, while FSRQ showed only a marginal correlation (with a chance probability of 8%). Without separating the source types, Kovalev (2009; 2009a) finds that the parsec-scale radio emission and the γ -ray flux are strongly related in the bright γ -ray objects of the LBAS sample. Similar results are found with the preliminary one-year *Fermi* sample by Giroletti et al. (2010).

Through our large sample of associations (230 sources) we can extend this correlation analysis in particular relying on the lower limiting flux (40 mJy) at the higher frequency (i.e. 20 GHz) of the AT20G survey. Fig. 4 shows that there is indeed a strong correlation between the radio flux at 20 GHz and the γ -ray flux (above 100 MeV) for the associations found from the cross correlation of the AT20G survey with the 1FGL/ILAC catalogue (§1).

Considering all the associations, the correlation has a rank correlation coefficient 0.53 and a chance probability of 10^{-17} . The

best fit of the correlation (shown by the solid line in Fig. 4) obtained with the least square bisector method (e.g. Isobe et al. 1990) has a slope 0.85 ± 0.04 . Fig. 4 shows that the population of blazars of unknown type (green filled circles) tends to have low radio fluxes, more similar to the distribution of BL Lacs (open blue circles in Fig. 4) in this plane. All AGNs (containing several source types – see §2), lie below the correlation (cyan open circles in Fig. 4), having lower γ -ray fluxes compared to FSRQs and BL Lacs. Due to the different redshift spanned by FSRQs and BL Lacs it is worth (Abdo et al. 2009; Mucke et al. 1997) to investigate this correlation separately for the two classes. Correlation analysis results are given in Tab. 1 where the Spearman correlation coefficient r_s and its chance probability P together with the correlation slope A are given.

We find significant correlations for FSRQs ($P = 3 \times 10^{-6}$), for BL Lacs ($P = 9.4 \times 10^{-6}$) and also for the blazars of unknown optical classification ($P = 1.9 \times 10^{-5}$). The slopes of all these three correlations are consistent at the 1σ level (last column in Tab. 1). Comparing to the results obtained from the LBAS sample (Abdo et al. 2009) we confirm the existence of a strong correlation between the radio and the γ -ray flux for BL Lacs while we find, for the first time, a similar strong correlation also for the population of FSRQs. The correlation found between the γ -ray and radio flux could be subject to possible biases related to the flux limits of the radio and γ -ray samples considered. Detailed study of possible selection effects is beyond the scope of the present work and requires numerical simulations. This will be the subject of a forthcoming paper.

For the 144 out of 230 associations found with sources with measured redshift we can also compare the distribution of FSRQ,

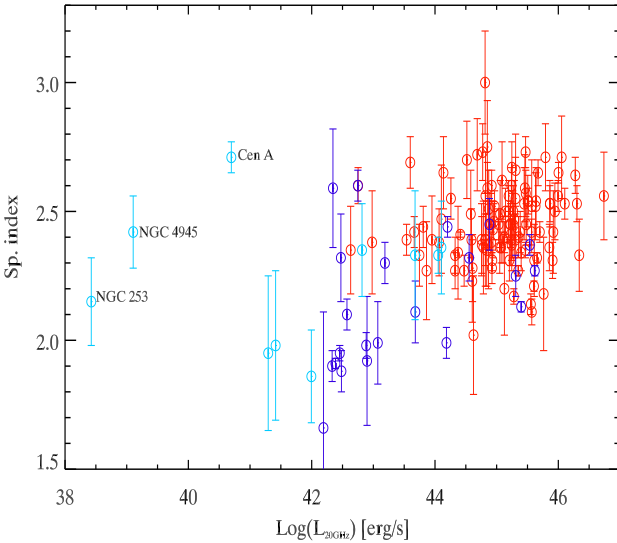


Figure 5. The photon γ -ray spectral index versus radio luminosity for the associations between the AT20G and the 1FGL sample which are also present in the 1LAC sample and have measured redshifts (144 sources). 112 FSRQs, 22 BL Lacs, 10 AGNs and 1 of unknown type are marked with red, blue and cyan symbols, respectively.

BL Lac and AGN in the plane of the γ -ray photon spectral index versus the radio luminosity (at 20 GHz). All the 112 FSRQs have a known redshift, while only 22 (out of 54) BL Lacs and all 10 sources classified AGNs have a known z . This is shown in Fig. 5.

It has been shown (Ghisellini, Tavecchio & Maraschi 2009) that FSRQs and BL Lacs tend to divide based on the γ -ray spectral index versus γ -ray luminosity. Here we see that also the in the spectral index – radio luminosity plane BL Lacs and FSRQ occupy different regions, with FSRQs being steeper and more luminous. Among the sources generically classified as AGN in the 1LAC sample we have marked in Fig. 5 the starburst NGC 253, the starburst/Seyfert 2 NGC 4945 and the radio galaxy Cen A which have lower radio luminosity with respect to FSRQs and BL Lacs.

However, considering that the number of associations with measured redshifts is only a fraction of the associations found, this plot is still highly incomplete, particularly for the population of BL Lacs.

In the AT20G sample 3795 sources have radio fluxes measured at 20, 8 and 5 GHz. In most of these cases, moreover, the measurements are at the same epoch. From these fluxes we can estimate the radio spectral index as $\alpha_{1-2} = \log(S_1/S_2)/\log(\nu_1/\nu_2)$, where $S_{i=1,2}$ is the flux measured at a certain frequency $\nu_{i=1,2}$. The high frequency (8–20 GHz) versus the low frequency (5–8 GHz) spectral index for the AT20G sample (grey dots) and of the 1FGL–AT20G associations are shown in Fig. 6. All blazars in the 1LAC sample associated with a counterpart in the AT20G sample have flat radio spectra: the average $\langle\alpha(5-8\text{GHz})\rangle = 0.02 \pm 0.28$ (1σ) and $\langle\alpha(8-20\text{GHz})\rangle = -0.16 \pm 0.27$ (1σ). There is no difference in the radio spectrum at low or high frequencies among the different blazar classes (FSRQ or BL Lac) and also the blazar candidates of unknown type (green filled circles in Fig. 6) have the same distribution in the $\alpha(5-8\text{GHz}) - \alpha(8-20\text{GHz})$ plane. This is indicative that in these sources we are observing the partially self-absorbed emission from a compact radio core.

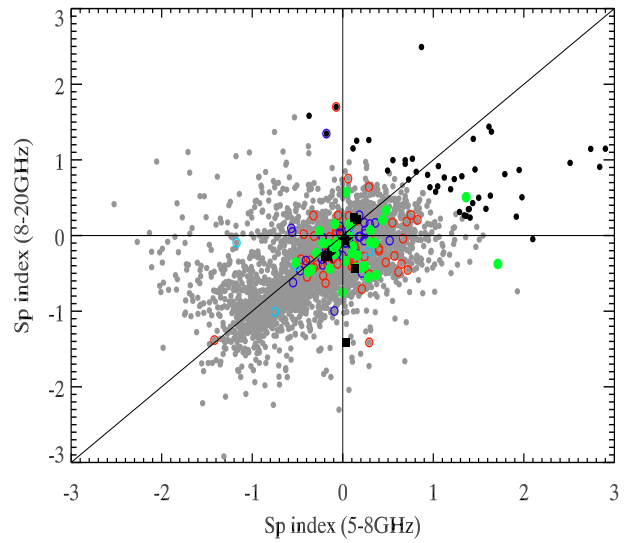


Figure 6. Low frequency (5–8 GHz) versus high frequency (8–20 GHz) spectral index for the 3795 AT20G sources with flux measurements at all the three frequencies. Black dots are the AT20G sources defined “Ultra-Inverted Spectrum” (UIS) which have $\alpha(5-20\text{GHz}) > +0.7$ (see Murphy et al. 2009). The open and filled symbols (same as Fig. 2) represent the associations found from the cross correlation of the AT20G sample and the *Fermi* 1FGL catalogue.

The AT20G survey contains $\sim 1.2\%$ of sources with extremely hard radio spectra, i.e. $\alpha(5-20\text{GHz}) > +0.7$ called “Ultra-Inverted Spectrum” (UIS) sources (black circles in Fig. 6). Among these sources we find 3 associations: one is the FSRQ PKS 0601–70 associated to 1FGL J0600.7–7037 and one is the BL Lac CRATES J1918–4111 associated to 1FGL J1918.4–4108. The third source, of the unknown class (i.e. the green circle among the UIS sources in Fig. 6), is PMN 1326–5256, associated with 1FGL J1327.0–5257. This source is particularly interesting, being the brightest radio source in the sub-sample of UIS. This source and its SED will be presented in Sec. 4. Fig. 6 shows that the sources detected by *Fermi* with a radio counterparts are not preferentially of the UIS type. In other words, being UIS does not give an extra chance to be a strong γ -ray blazar.

4 SPECTRAL CLASSIFICATION OF NEW BLAZAR CANDIDATES

From the cross correlation of the AT20G and the 1FGL catalogues we found 46 associations which are classified as blazars (i.e. present in the 1LAC sample) but of unknown type. For these sources it is important to find some possible evidences that might lead to their classification as either BL Lac or FSRQ. Similarly we have found 8 new associations. Several diagnostics are used for the classification of blazars, the main one relies on their optical spectra. Different classification criteria exist: in the 1LAC sample a BL Lac should show no or weak lines (equivalent width $< 5\text{ \AA}$) and the Ca II H/K ratio < 0.4 (A10a).

Another approach is to build the broad band SED and compare it with those of the two classes (FSRQ and BL Lac) to possibly identify similar signatures. We also model the SED, adopting the modelling of Ghisellini et al. (2009).

An on-going project is to study the 46 associations of unknown type in order to classify them. Here we present, as a first result, one of these sources, 1FGL 1327.0–5257 (associated to PMN J1326–5256 and to the AT20G J132649–525623) which is the source with the highest radio flux density of the UIS class.

Among the 8 new associations we searched for any *Swift* pointing containing these sources. In two cases (1FGL J0904.7–3514 and 1FGL J1656.2–3257) there are *Swift* observations of the field. We associate 1FGL J1656.2–3257 with the Swift J1656.3–3302 already classified as a FSRQ at $z \sim 2.4$ (Masetti et al. 2008) and we present here its broad band SED by combining the published data, the XRT data and the Fermi ones. We also build the SED of 1FGL J0904.7–3514 and we classify it as a FSRQ.

The *Swift* data were analysed with the software distributed as part of the Heasoft v. 6.7 and the calibration database updated to September 2009 was adopted. The XRT data were processed with the standard procedure. We considered photon counting (PC) mode data with the standard 0–12 grade selection. Source events were extracted in a circular region of aperture $\sim 47''$, and background was estimated in a same sized circular region far from the source. Response matrices were created through the `xrtmkarf` task. The channels with energies below 0.3 keV and above 10 keV were excluded from the fit. The spectra were analysed through XSPEC(v11.3.2ag) with an absorbed power law with a fixed Galactic column density (Kalberla et al. 2005).

UVOT (Roming et al. 2005) source counts were extracted from a circular region 5''-sized centred on the source position, while the background was extracted from a larger nearby source-free region. Data were integrated with the `uvotimsum` task and then analysed through the `uvotsource` task. The observed magnitudes have been dereddened according to the formulae by Cardelli et al. (1989) and converted into fluxes by using standard formulae and zero points from Poole et al. (2008).

4.0.1 1FGL J0904.7–3514

The *Fermi* source centroid is at RA=136.195° and Dec=−35.248° with a 68% uncertainty radius (almost circular) of 0.06°. There are three *Swift* pointings containing this position: one performed on 15–06–2009 (~ 5 ks) and two in January 2010 (of ~ 6 and 7 ks). The *Fermi* 1FGL J0904.7–3514 source has a γ -ray flux (averaged over the 11 months survey and integrated above 100 MeV) of 7.6×10^{-8} phot $\text{cm}^{-2} \text{s}^{-1}$ and its photon spectral index is 2.69 ± 0.1 . Our cross correlation of the AT20G catalogue with the 1FGL associated this source with AT20G J090442–351423, which is ~ 1 arcmin distant from the *Fermi* centroid.

By summing all the *Swift* XRT images (Fig. 7) we find within the 68% error ellipse of the *Fermi* source a bright X-ray source coincident with AT20GJ090442–35142 (source A in Fig. 7). By searching in NED for the possible other sources present in this field we found that there is PMN J0904–3514 that was one of the possible 5 counterparts of the source 3EGJ0903–3531 (Mattox et al. 2001) and it is closer to the *Fermi* centroid (source B - dashed ellipse in Fig. 7). However, the possible X-ray counterpart of source B (which is located at the border of its error ellipse) is a factor 10 fainter than source A which we claim is the X-ray and coincident radio counterpart of the *Fermi* 1FGL J0904.7–3514.

In Fig. 8 we show the SED of 1FGL J0904.7–3514 obtained combining the *Fermi* data and the X-ray and Optical/UV data available (red symbols). For comparison we also show (green symbols) the X-ray and optical data of source B in the field, i.e. PMN J0904–3514. We see that the SED of the association 1FGL J0904.7–3514

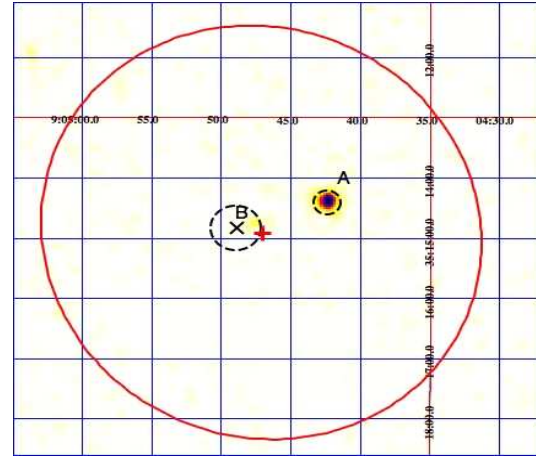


Figure 7. XRT image of 1FGL J0904.7–3514. The *Fermi*/LAT centroid (marked with the plus sign) and its 68% error ellipse is shown (solid red line). The bright X-ray source (labelled A) is coincident with the position of the radio AT20G source AT20GJ090442–35142 (marked by the black dashed circle). The position of the other source within the field, PMN J0904–3514 (labelled B) is shown by the dashed ellipse.

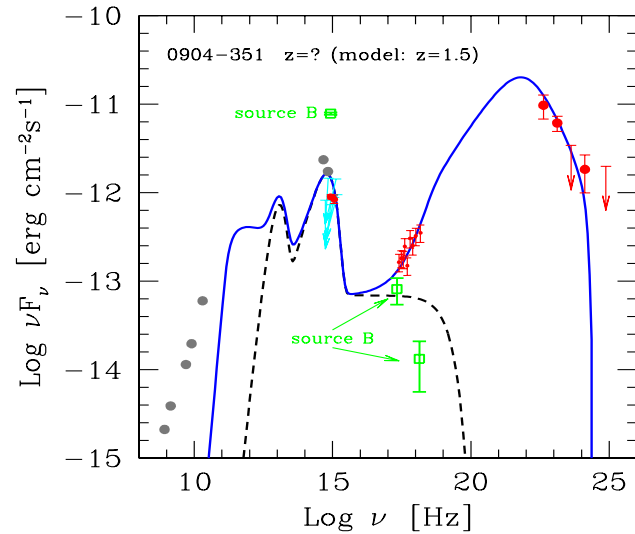


Figure 8. SED of 1FGL J0904.7–3514. Red points are XRT and UVOT data and at high energies the *Fermi* LAT data taken from the 1FGL catalogue. The green points are the XRT and UVOT data of the other source within the *Fermi* 68% confidence ellipse (which is not present in the AT20G sample). Radio data are from the AT20G survey (at 5, 8 and 20 GHz) and other data are collected from the literature.

with AT20G J090442–35142 (source A) can be well modelled as a typical blazar with a model redshift $z \sim 1.5$ while the other source has a very steep X-ray spectrum inconsistent with the *Fermi* data.

4.0.2 1FGL J1656.2–3257

The *Fermi* source centroid is at RA=254.055 and Dec=−32.9513 with a 68% confidence ellipse almost circular with radius 0.07°. Within this region there is AT20G J165616–330207 which is at a separation of 0.085° and has an association probability of

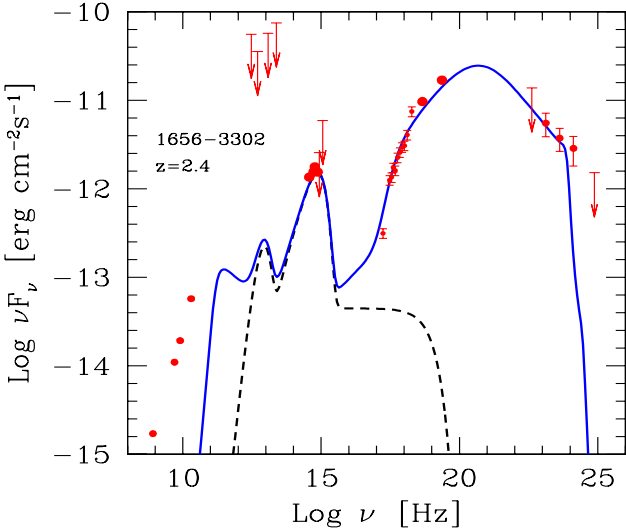


Figure 9. SED of 1FGL J1656.2–3257.

94%. The *Fermi* 1FGL J1656.2–3257 has a photon spectral index $\Gamma=2.43\pm0.11$ and a γ -ray flux (averaged over the 11 months survey and integrated above 100 MeV) of 5.81×10^{-8} phot $\text{cm}^{-2} \text{s}^{-1}$. The position of the radio counterpart AT20G J165616–330207 that we associate with the *Fermi* one is coincident with the *Swift* source SWIFT J1656–3302 (Bird et al. 2007; Malizia et al. 2007; Krivonos et al. 2007; Bodaghee et al. 2007; Sazonov et al. 2007). This source was classified as a FSRQ at redshift $z \sim 2.4$ (Masetti et al. 2008). There are two *Swift* pointings of SWIFT J1656–3302 in June 2006 (with an exposure of ~ 4.3 ks and 4.8 ks). We used these observations to build the SED shown in Fig. 9, collecting the other data from Masetti et al. (2008). Also in this case the source appears to be well modelled by the typical SED of a FSRQ.

4.0.3 IFGL J1327–5257

The *Fermi* centroid is at RA=201.75° and Dec=−52.96° with an error radius of 0.04°. We associate this source to the AT20G J132649–525623. The *Fermi* source is already associated in the 1LAC sample to PMN J1326–5256 which is coincident with the AT20G source that we associated with the 1FGL one. The γ -ray flux of the *Fermi* source, integrated above 100 MeV is 6.6×10^{-8} phot $\text{cm}^{-2} \text{s}^{-1}$ and the photon spectral index is 2.32 ± 0.06 .

PMN J1326–5256 is a compact radio source with scarce data in the literature. The AT20G counterpart is the brightest source at 20 GHz among the class of “Ultra-Inverted Spectrum” (UIS) in this survey. It is detected at a flux level of 2.061 ± 0.1 , 1.350 ± 0.07 and 0.606 ± 0.03 Jy at 20 GHz, 8 GHz and 5 GHz, respectively, with a spectral index $\alpha(5, 20 \text{ GHz})=+0.8\pm0.07$ ($F(\nu) \propto \nu^\alpha$).

This source is intriguing in many aspects. Its redshift is unknown but its classification as a FSRQ seems to be excluded by Bignall et al. (2008) based on its featureless spectrum (in the 5000–9100 Å band).

The source has no large scale structure at 2.3 GHz, being unresolved at the level of 16 mas resolution of ATCA and AT-LBA (Bingall et al. 2008). Its radio properties have been extensively monitored (Cimó et al. 2006) because of its intra-day variability.

There are three *Swift* observations of J1326–5256: two in Au-

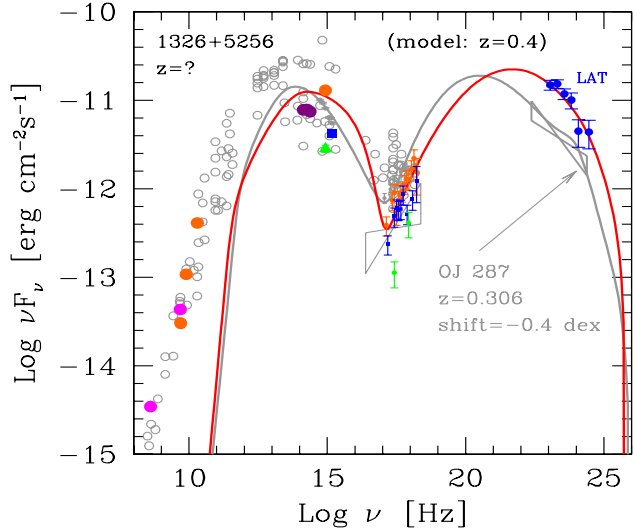


Figure 10. SED of J1326–5256 (coloured symbols). The radio data at 408 MHz and 4.85 GHz are shown with the magenta filled circles, while the AT20G fluxes (at 5, 8 and 20 GHz) are show by the orange circles. 2MASS J, H, K data are shown with the black symbols. The red, blue, green symbols correspond to the three *Swift* observations. The open grey circles and grey bows represent the data of OJ287 (from Ghisellini et al. 2009, Tavecchio et al. 2010) and the grey solid line is the best fit model, scaled in flux by a factor 0.4 dex. The solid blue line is the best fit model to SED of J1326–5256.

gust 2009 and one in October 2009. Fig. 10 shows the SED of J1326–5256 with all the available data (coloured symbols). For comparison we also report the data of the classic BL Lac OJ 287 (grey symbols) shifted in flux by a factor 0.4 dex. The two models (blue and grey solid lines) represent the fit with the model described in Ghisellini & Tavecchio (2009). The close similarity of the two SEDs leads us to propose that J1326–5256 is a BL Lac. If it is slightly weaker than OJ 287 (that has $z = 0.306$) because it is more distant, than the redshift of J1326–5256 is $z \sim 0.4$.

5 CONCLUSIONS

In this paper we cross correlated the *Fermi* 1FGL catalog (A10) containing the sources detected above 100 MeV during the 11 months survey with a complete sample of radio sources selected by the AT20G survey in the southern hemisphere with 20 GHz flux density larger than 40 mJy. The cross correlation led to identify highly probable (association probability $>80\%$) radio counterparts for 230 1FGL sources. 222 of these are already classified as blazars in the 1LAC catalog (A10a) and 8 sources are new associations.

Using the sample of the associated sources and considering the uniform radio flux measurement of the AT20G survey, we have studied the radio to γ -ray flux correlation among different blazar sub-classes finding that there is a significant correlation between these two fluxes both for BL Lacs and for FSRQs. Such a correlation has a slope of ~ 0.85 for both blazars sub-classes. If this correlation is further confirmed in the future by the extension of the sample of *Fermi* blazars with measured radio fluxes, it would

RA deg	Dec deg	P	Sep arcmin	1FGL	AT20G	
116.613	-07.164	0.97	2.70	J0746.5-0711	J074627-070951	Bird, et al., 2007, ApJS 170, 17
136.176	-35.239	0.99	1.07	J0904.7-3514	J090442-351423	Bodaghee et al. 2007, A&A 467, 585
188.529	-57.598	0.99	1.18	J1234.0-5736	J123407-573552	Cardelli, J. A., et al., ApJ, 345, 245
194.020	-59.328	0.98	3.06	J1256.1-5922	J125604-591943	Cimo' et al. 2006, PoS
198.767	-53.576	0.98	3.77	J1314.9-5338	J131504-533436	Ghisellini, G., Tavecchio F., & Maraschi, L., 2009, MNRAS, 396, L105
254.070	-33.035	0.94	5.10	J1656.2-3257	J165616-330207	Ghisellini, G. & Tavecchio, F., 2009, MNRAS, 397, 985
262.945	-30.052	0.90	7.07	J1732.0-2957	J173146-300309	Giroletti, M. et al., 2010, 009 Fermi Symposium, arXiv:1001.5123
275.910	-34.903	0.99	0.93	J1823.5-3454	J182338-345412	Gliozzi M. et al., 2008, A&A, 478, 723
						Healey, S. E., et al., 2007, ApJS, 171, 61
						Healey, S. E., et al., 2008, ApJS, 175, 97
						Isobe, T., et al., 1990, ApJ, 364, 104
						Kalberla, P. M. W., et al., 2005, A&A, 440, 775
						Krionos et al. 2007, A&A 475, 775
						Kovalev, Y. Y., et al. 2009, ApJ, 707, L56
						Kovalev, Y. Y., et al., 2009a, ApJ, 696, L17
						Lenc E. & Tingay S.J., 2009, AJ, 137, 537
						Malizia et al. 2007, ApJ, 668, 81
						Masetti N., et al., 2008, A&A, 480, 715
						Massaro, E., et al., 2009, A&A, 495, 691
						Mattox, J. R., Hartman, R. C., Reimer, O., 2001, ApJS, 135, 155
						Murphy, T., et al., 2010, MNRAS, 402, 2403
						Mucke et al. 1997, A&A, 320, 33
						Poole, T. S., et al., 2008, MNRAS, 383, 627
						Roming et al., 2005, Space Science Reviews, 120, 3, 95
						Sazonov et al. 2007, A&A 462, 57
						Stecker F. W., Salamon M. H., Malkan M. A., 1993, ApJ, 410, L71
						Sutherland, W. & Saunders, W., 1992, MNRAS, 259, 413
						Tavecchio F. et al., 2010, MNRAS, 401, 1570
						Taylor et al. 2007, ApJ, 671, 1355

Table 2. The eight new associations found by the cross-correlation of the 1FGL sample and the AT20G survey. Positions (RA and Dec) of the associated radio source, probability of the association and angular separation between the AT20G counterpart and the 1FGL centroid are reported. The two sources (J0904 classified as FSRQ in this paper) whose SED is studied in this work are marked in boldface.

help to correctly estimate the contribution of blazars to the γ -ray background (e.g. Stecker et al. 1993).

The radio properties of the 230 associations show also that they are typically flat spectrum radio sources. In particular, steep spectrum radio sources are not the radio counterparts to *Fermi* sources, but also radio sources with extremely hard radio spectra (i.e. $\alpha(5-20 \text{ GHz}) > +0.7$) which are the 1.2% of the AT20G sample are not preferentially detected by *Fermi*. Indeed, we find only three associations with such hard radio sources.

We have presented the spectral energy distribution of three sources: two (1FGL J0904.7-3514 and 1FGL J1656.2-3257) are among the eight new associations that we have found by cross correlating the *Fermi* sample and the AT20G survey. Their spectrum, obtained by combining radio, *Swift* and *Fermi* data resembles that of a typical FSRQ. The third source (1FGL J1327-5257) is presented as a first interesting result of an on-going program aimed at studying and classify the unknown blazar candidates of the 1LAC sample. This source is among the brightest radio sources in the AT20G survey and it is characterised by a rapidly variable radio emission. Its SED is remarkably similar to that of the prototypical BL Lac OJ 287, but located at the slightly greater redshift $z \sim 0.4$.

ACKNOWLEDGMENTS

This work was partly financially supported by a 2007 COFIN-MIUR grant and ASI I/088/06/0 grant. This research has made use of the NASA/IPAC Extragalactic Database (NED) which is operated by the Jet Propulsion Laboratory, California Institute of Technology, under contract with the National Aeronautics and Space Administration. This work is based on the public available data of the *Swift* satellite and *Fermi* LAT instrument obtained through the HEASARC.

REFERENCES

- Abdo, A. A., et al., 2009, ApJ 700, 597
- Abdo A.A. et al., 2009a, ApJ, 707, L142
- Abdo, A. A., et al. 2010, ApJS subm., arXiv:1002.2280 (A10)
- Abdo, A. A., et al. 2010a, ApJ subm., arXiv:1002.0150 (A10a)
- Abdo A. A. et al., 2010b, ApJ, 709, L152
- Atwood, W. B., et al., 2009, ApJ, 697, 1071
- Bignall et al., 2008, arXiv:0805.3891

RA deg	Dec deg	P	Sep arcmin	AT20G	1FGL	ILAC	Class	Clean
0.325	-7.774	0.94	5.32	J000118-074626	J0000.9-0745	CRATES J0001-0746	BLL	Y
1.148	-47.605	0.97	1.92	J000435-473619	J0004.7-4737	PKS 0002-478	FSRQ	Y
3.249	-39.907	0.98	2.67	J001259-395426	J0013.1-3952	PKS 0010-401	BLL	Y
4.399	-5.2115	0.98	2.42	J001735-051241	J0017.4-0510	CGRABS J0017-0512	FSRQ	Y
7.572	-42.412	0.94	4.72	J003017-422446	J0029.9-4221	PKS 0027-426	FSRQ	Y
9.561	-24.983	0.92	6.03	J003814-245901	J0038.4-2504	PKS 0035-252	FSRQ	Y
11.887	-25.288	0.94	5.84	J004733-251717	J0047.3-2512	NGC 253	AGN ^(a)	Y
12.497	-57.641	0.99	1.14	J004959-573827	J0049.8-5738	PKS 0047-579	FSRQ	Y
12.589	-4.872	0.90	7.17	J005021-045221	J0050.0-0446	PKS 0047-051	FSRQ	Y
12.672	-9.484	0.99	0.46	J005041-092905	J0050.6-0928	PKS 0048-09	BLL	Y
12.784	-6.834	0.99	0.96	J005108-065004	J0051.1-0649	PKS 0048-071	FSRQ	Y
14.509	-32.572	0.98	4.69	J005802-323420	J0058.4-3235	PKS 0055-328	BLL	Y
19.052	-11.604	0.81	10.9	J011612-113614	J0115.5-1132	PKS 0113-118	FSRQ	Y
19.738	-21.691	0.87	4.96	J011857-214130	J0118.7-2137	PKS 0116-219	FSRQ	Y
20.132	-27.023	0.99	0.46	J012031-270124	J0120.5-2700	PKS 0118-272	BLL	Y
23.181	-16.913	0.99	1.34	J013243-165448	J0132.6-1655	PKS 0130-17	FSRQ	Y
24.409	-24.514	0.98	2.20	J013738-243053	J0137.5-2428	PKS 0135-247	FSRQ	Y
25.407	-9.500	0.99	1.32	J014137-093001	J0141.7-0929	PKS 0139-09	BLL	Y
26.264	-27.559	0.98	2.04	J014503-273333	J0144.9-2732	PKS 0142-278	FSRQ	Y
29.463	-46.239	0.96	3.67	J015751-461423	J0157.5-4613	CGRABS J0157-4614	FSRQ	Y
29.658	-39.534	0.92	7.02	J015838-393204	J0158.0-3931	CGRABS J0158-3932	BLL	Y
29.930	-27.677	0.97	1.11	J015943-274038	J0159.7-2741	CRATES J0159-2740	BLL	Y
31.240	-17.022	0.98	1.52	J020457-170120	J0205.0-1702	PKS 0202-17	FSRQ	Y
32.692	-51.017	0.99	0.98	J021046-510101	J0210.6-5101	PKS 0208-512	BLL	Y
34.261	-8.347	0.87	8.43	J021702-082052	J0217.0-0829	PKS 0214-085	FSRQ	Y
35.503	-16.254	0.95	4.09	J022200-161516	J0222.1-1618	PKS 0219-164	FSRQ	Y
37.368	-36.732	0.99	1.26	J022928-364356	J0229.3-3644	PKS 0227-369	FSRQ	Y
40.669	-0.012	0.97	8.75	J024240-000046	J0242.7+0007	RX J0241.9+0009	UNKNOWN	N
41.500	-46.854	0.99	1.17	J024600-465116	J0245.9-4652	PKS 0244-470	FSRQ	Y
43.199	-22.323	0.99	0.54	J025247-221924	J0252.8-2219	PKS 0250-225	FSRQ	Y
44.420	-12.200	0.89	8.19	J025740-121201	J0257.8-1204	CGRABS J0257-1212	FSRQ	Y
45.961	-62.190	0.97	2.91	J030350-621125	J0303.4-6209	PKS 0302-623	FSRQ	Y
45.860	-24.119	0.99	1.62	J030326-240711	J0303.5-2406	PKS 0301-243	BLL	Y
47.483	-60.977	0.98	1.51	J030956-605839	J0310.1-6058	PKS 0308-611	FSRQ	Y
48.987	-10.527	0.99	1.61	J031556-103138	J0315.9-1033	PKS 0313-107	FSRQ	Y
51.344	-56.484	0.97	3.33	J032522-562905	J0325.6-5626	CRATES J0325-5635	UNKNOWN	N
53.556	-40.140	0.99	1.66	J033413-400825	J0334.2-4010	PKS 0332-403	BLL	Y
53.564	-37.428	0.98	2.89	J033415-372543	J0334.4-3727	CRATES J0334-3725	BLL	Y
54.807	-17.600	0.99	1.58	J033913-173600	J0339.1-1734	PKS 0336-177	AGN	Y
54.878	-1.776	0.96	5.69	J033930-014635	J0339.2-0143	PKS 0336-01	FSRQ	N
55.830	-25.504	0.92	6.23	J034319-253017	J0343.4-2536	PKS 0341-256	FSRQ	Y
57.158	-27.820	0.96	2.44	J034838-274913	J0348.5-2751	PKS 0346-279	FSRQ	Y
57.490	-21.046	0.99	2.08	J034957-210247	J0349.9-2104	PKS 0347-211	FSRQ	Y
59.251	-49.929	0.87	6.49	J035700-495547	J0357.1-4949	PKS 0355-500	BLL	Y
60.503	-26.261	0.97	3.37	J040200-261540	J0402.1-2618	CRATES J0402-2615	UNKNOWN	Y
60.974	-36.083	0.99	1.21	J040353-360500	J0403.9-3603	PKS 0402-362	FSRQ	Y
61.391	-13.137	0.98	2.33	J040534-130813	J0405.6-1309	1WGA J0405.6-1313	AGN	N
61.745	-38.440	0.81	5.74	J040658-382627	J0407.4-3827	PKS 0405-385	FSRQ	Y
63.305	-53.533	0.92	3.37	J041313-533200	J0413.4-5334	CRATES J0413-5332	FSRQ	Y
64.152	-18.852	0.98	0.84	J041636-185108	J0416.5-1851	PKS 0414-189	FSRQ	Y
65.544	-6.729	0.96	4.06	J042210-064344	J0422.0-0647	CRATES J0422-0643	FSRQ	Y
65.815	-1.342	0.99	2.23	J042315-012033	J0423.2-0118	PKS 0420-01	FSRQ	Y
67.168	-37.938	0.99	0.56	J042840-375619	J0428.6-3756	PKS 0426-380	BLL	Y
68.533	-20.254	0.96	3.13	J043408-201517	J0434.1-2018	CRATES J0434-2015	BLL	Y
69.645	-12.851	0.97	3.29	J043834-125103	J0438.8-1250	PKS 0436-129	FSRQ	Y
70.660	-0.295	0.99	2.20	J044238-001744	J0442.7-0019	BZB J0442-0018	BLL	N
71.256	-60.250	0.88	6.29	J044501-601500	J0445.2-6008	J0445-6015	AGN	N
72.353	-43.835	0.99	1.10	J044924-435008	J0449.5-4350	PKS 0447-439	BLL	Y
73.311	-28.127	0.98	2.42	J045314-280737	J0453.2-2805	PKS 0451-28	FSRQ	Y
73.961	-46.266	0.98	3.06	J045550-461558	J0455.6-4618	PKS 0454-46	FSRQ	Y
74.152	-31.603	0.97	4.33	J045636-313611	J0456.4-3132	CRATES J0456-3136	FSRQ	Y
74.263	-23.414	0.99	0.54	J045703-232451	J0457.0-2325	PKS 0454-234	FSRQ	Y
75.303	-1.987	0.97	1.98	J050112-015914	J0501.0-0200	PKS 0458-02	FSRQ	Y
76.463	-4.323	0.91	3.39	J050551-041926	J0505.8-0416	CRATES J0505-0419	FSRQ	Y
76.977	-61.078	0.94	4.33	J050754-610442	J0507.3-6103	PKS 0506-61	FSRQ	N
79.187	-62.118	0.99	0.81	J051644-620706	J0516.7-6207	PKS 0516-621	UNKNOWN	Y

RA deg	Dec deg	P	Sep arcmin	AT20G	1FGL	ILAC	Class	Clean
80.741	-36.458	0.90	5.19	J052257-362730	J0522.8-3632	PKS 0521-36	BLL	Y
81.569	-48.510	0.98	1.76	J052616-483036	J0526.3-4829	PKS 0524-485	FSRQ	Y
83.418	-83.410	0.99	1.07	J053340-832439	J0533.0-8324	PKS 0541-834	FSRQ	Y
84.709	-44.085	0.99	0.47	J053850-440508	J0538.8-4404	PKS 0537-441	BLL	Y
84.975	-28.665	0.80	12.3	J053954-283956	J0539.1-2847	PKS 0537-286	FSRQ	Y
84.814	-3.949	0.90	5.22	J053915-035657	J0539.4-0400	CRATES J0539-0356	UNKNOWN	N
89.526	-38.641	0.83	8.94	J055806-383830	J0557.6-3831	CRATES J0558-3838	BLL	Y
89.693	-74.985	0.97	2.38	J055846-745906	J0559.2-7500	PKS 0600-749	BLL	Y
90.297	-70.602	0.95	2.59	J060111-703609	J0600.7-7037	PKS 0601-70	FSRQ	Y
92.006	-15.343	0.99	0.65	J060801-152036	J0608.0-1521	CRATES J0608-1520	UNKNOWN	Y
91.942	-6.385	0.82	9.30	J060746-062307	J0608.1-0630c	CRATES J0609-0615	UNKNOWN	N
91.998	-8.580	0.96	3.93	J060759-083449	J0608.2-0837	PKS 0605-08	FSRQ	Y
94.389	-17.256	0.96	3.82	J061733-171525	J0617.7-1718	CRATES J0617-1715	BLL	Y
96.703	-54.537	0.87	7.94	J062648-543214	J0625.9-5430	CGRABS J0625-5438	FSRQ	Y
96.533	-42.892	0.94	6.26	J062607-425332	J0626.6-4254	CRATES J0626-4253	UNKNOWN	Y
96.778	-35.487	0.99	2.76	J062706-352916	J0627.3-3530	PKS 0625-35	AGN ^(c)	Y
97.349	-19.988	0.97	3.50	J062923-195919	J0629.6-2000	PKS 0627-199	BLL	Y
97.748	-24.112	0.99	0.35	J063059-240645	J0630.9-2406	CRATES J0630-2406	BLL	Y
98.943	-75.271	0.95	5.09	J063546-751616	J0636.1-7521	PKS 0637-75	FSRQ	Y
102.118	-17.734	0.93	5.53	J064828-174405	J0648.7-1740	TXS 0646-176	FSRQ	N
102.602	-16.627	0.95	4.52	J065024-163739	J0650.6-1635	PKS 0648-16	UNKNOWN	N
105.129	-66.179	0.99	0.92	J070031-661045	J0700.4-6611	PKS 0700-661	UNKNOWN	Y
105.393	-46.576	0.81	7.77	J070134-463436	J0702.0-4628	PKS 0700-465	FSRQ	Y
105.678	-19.855	0.90	7.24	J070242-195121	J0702.2-1954	TXS 0700-197	UNKNOWN	N
111.460	-0.915	0.98	2.56	J072550-005457	J0725.9-0053	PKS 0723-008	BLL	N
112.58	-11.687	0.99	0.75	J073019-114113	J0730.3-1141	PKS 0727-11	FSRQ	N
113.680	-77.187	0.94	4.66	J073443-771114	J0734.1-7715	PKS 0736-770	UNKNOWN	Y
118.610	-11.787	0.99	0.53	J075426-114716	J0754.4-1147	OI -187	UNKNOWN	N
121.790	-5.687	0.95	3.44	J080709-054115	J0807.0-0544	PKS 0804-05	UNKNOWN	Y
122.064	-7.852	0.99	0.99	J080815-075110	J0808.2-0750	PKS 0805-07	FSRQ	Y
122.763	-75.507	0.97	2.51	J081103-753027	J0811.1-7527	CRATES J0811-7530	UNKNOWN	Y
123.548	-10.203	0.89	5.72	J081411-101210	J0814.5-1011	AT20G J0814-1012	UNKNOWN	N
124.457	-9.558	0.91	6.75	J081749-093330	J0818.0-0938	CGRABS J0817-0933	BLL	Y
126.506	-22.507	0.98	2.16	J082601-223027	J0825.8-2230	PKS 0823-223	BLL	N
126.464	-32.306	0.98	2.12	J082551-321823	J0825.9-3216	PKS 0823-321	UNKNOWN	N
131.26	-54.969	0.98	1.22	J084502-545808	J0845.0-5459	PMN J0845-5458	UNKNOWN	N
131.756	-23.617	0.98	2.50	J084701-233701	J0846.9-2334	CRATES J0847-2337	UNKNOWN	Y
132.440	-35.683	0.97	1.40	J084945-354101	J0849.6-3540	VCS2 J0849-3541	UNKNOWN	N
132.539	-12.226	0.99	1.38	J085009-121337	J0850.0-1213	CGRABS J0850-1213	FSRQ	Y
134.173	-11.087	0.99	0.42	J085641-110514	J0856.6-1105	CGRABS J0856-1105	UNKNOWN	Y
136.222	-57.584	0.98	2.44	J090453-573504	J0905.1-5736	PKS 0903-57	FSRQ	N
137.437	-2.524	0.99	2.65	J090944-023129	J0909.6-0229	PKS 0907-023	FSRQ	Y
148.261	-8.671	0.99	1.58	J095302-084018	J0953.0-0838	CRATES J0953-0840	BLL	Y
152.715	-2.005	0.95	4.99	J101051-020019	J1011.0-0156	CRATES J1010-0200	FSRQ	Y
156.640	-85.720	0.89	2.50	J102633-854315	J1028.7-8543	PKS 1029-85	UNKNOWN	Y
164.679	-80.064	0.98	3.28	J105843-800353	J1058.1-8006	PKS 1057-79	BLL	Y
164.801	-11.572	0.97	3.37	J105912-113422	J1059.3-1132	PKS B1056-113	BLL	Y
165.968	-53.950	0.99	1.15	J110352-535700	J1103.9-5355	PKS 1101-536	UNKNOWN	N
170.354	-5.899	0.99	1.63	J112125-055356	J1121.5-0554	PKS 1118-05	FSRQ	Y
170.831	-64.293	0.97	3.53	J112319-641735	J1122.9-6415	PMN J1123-6417	UNKNOWN	N
171.381	-35.950	0.97	2.88	J112531-355703	J1125.5-3559	CRATES J1125-3557	UNKNOWN	Y
171.768	-18.955	0.97	3.99	J112704-185719	J1126.8-1854	PKS 1124-186	FSRQ	Y
172.529	-14.824	0.98	2.35	J113007-144927	J1130.2-1447	PKS 1127-14	FSRQ	N
176.756	-38.202	0.99	0.65	J114701-381210	J1146.9-3812	PKS 1144-379	FSRQ	Y
176.965	-7.410	0.98	2.87	J114751-072438	J1147.7-0722	PKS 1145-071	FSRQ	Y
178.072	-8.684	0.93	4.26	J115217-084103	J1152.2-0836	PKS B1149-084	FSRQ	Y
178.942	-81.021	0.84	9.22	J115546-810117	J1153.4-8108	PMN-CA J1149-8112	UNKNOWN	N
178.525	-32.712	0.98	2.49	J115406-324243	J1154.2-3242	PKS 1151-324	UNKNOWN	Y
179.794	-21.834	0.96	4.38	J115910-215005	J1159.4-2149	PKS 1157-215	FSRQ	N
181.07	-7.169	0.96	4.31	J120416-071009	J1204.3-0714	CRATES J1204-0710	BLL	Y
181.389	-26.568	0.93	6.55	J120533-263404	J1205.9-2637	PKS 1203-26	FSRQ	Y
191.695	-25.796	0.98	2.21	J124646-254749	J1246.7-2545	PKS 1244-255	FSRQ	Y
194.046	-5.789	0.99	0.43	J125611-054721	J1256.2-0547	3C 279	FSRQ	Y
194.066	-11.776	0.94	4.50	J125615-114635	J1256.5-1148	CRATES J1256-1146	UNKNOWN	Y
194.659	-18.000	0.95	3.91	J125838-180001	J1258.4-1802	PKS B1256-177	FSRQ	Y
194.727	-22.325	0.96	3.27	J125854-221930	J1258.7-2221	PKS 1256-220	FSRQ	Y

RA deg	Dec deg	P	Sep arcmin	AT20G	1FGL	ILAC	Class	Clean
195.917	-46.350	0.92	4.48	J130340-462103	J1304.0-4622	CGRABS J1303-4621	FSRQ	Y
196.364	-49.467	0.99	0.24	J130527-492804	J1305.4-4928	NGC 4945	AGN ^(b)	Y
197.071	-67.117	0.86	7.72	J130817-670704	J1307.3-6701	PKS 1304-668	UNKNOWN	N
199.033	-33.649	0.98	2.60	J131608-333858	J1316.1-3341	PKS 1313-333	FSRQ	Y
200.653	-9.615	0.93	6.57	J132236-093655	J1322.7-0943	OP -034	FSRQ	Y
201.365	-43.018	0.98	2.20	J132527-430104	J1325.6-4300	CEN A	AGN	Y
201.705	-52.939	0.99	2.38	J132649-525623	J1327.0-5257	PMN J1326-5256	UNKNOWN	N
202.254	-56.134	0.98	3.32	J132901-560802	J1329.2-5605	PMN J1329-5608	UNKNOWN	N
202.545	-70.053	0.96	4.29	J133010-700313	J1330.7-7006	PKS 1326-697	UNKNOWN	N
203.018	-5.162	0.96	3.53	J133204-050944	J1331.9-0506	PKS 1329-049	FSRQ	Y
203.163	-12.937	0.99	0.32	J133239-125616	J1332.6-1255	CRATES J1332-1256	FSRQ	Y
204.415	-12.956	0.99	1.98	J133739-125724	J1337.7-1255	PKS 1335-127	FSRQ	Y
206.060	-17.395	0.99	0.63	J134414-172342	J1344.2-1723	CGRABS J1344-1723	FSRQ	Y
206.919	-37.843	0.97	2.36	J134740-375037	J1347.8-3751	CRATES J1347-3750	FSRQ	Y
208.694	-10.684	0.99	1.86	J135446-104103	J1354.9-1041	PKS 1352-104	FSRQ	Y
210.174	-56.082	0.93	5.47	J140041-560455	J1400.9-5559	PMN J1400-5605	UNKNOWN	N
211.915	-43.042	0.95	5.73	J140739-430231	J1407.5-4256	CGRABS J1407-4302	UNKNOWN	Y
212.235	-7.873	0.99	1.43	J140856-075225	J1408.9-0751	PKS 1406-076	FSRQ	Y
216.984	-42.105	0.97	4.33	J142756-420618	J1428.2-4204	PKS 1424-41	FSRQ	Y
220.988	-39.144	0.99	1.87	J144357-390839	J1444.0-3906	PKS 1440-389	BLL	Y
224.361	-35.653	0.99	1.52	J145726-353910	J1457.5-3540	PKS 1454-354	FSRQ	Y
226.258	-34.545	0.97	3.36	J150502-343242	J1505.1-3435	CRATES J1505-3432	UNKNOWN	Y
227.723	-5.718	0.96	4.69	J151053-054307	J1511.1-0545	PKS 1508-05	FSRQ	Y
228.210	-9.099	0.99	0.30	J151250-090558	J1512.8-0906	PKS 1510-08	FSRQ	Y
228.667	-47.808	0.93	6.36	J151440-474828	J1514.1-4745	PMN J1514-4748	UNKNOWN	N
229.424	-24.372	0.99	1.78	J151741-242220	J1517.8-2423	AP LIB	BLL	Y
230.657	-27.503	0.98	2.67	J152237-273011	J1522.6-2732	PKS 1519-273	BLL	Y
238.381	-24.368	0.98	3.21	J155331-242206	J1553.4-2425	PKS 1550-242	UNKNOWN	Y
238.389	-31.308	0.99	2.25	J155333-311832	J1553.5-3116	AT20G J1553-3118	BLL	N
240.961	-49.068	0.99	0.42	J160350-490405	J1603.8-4903	PMN J1603-4904	UNKNOWN	N
241.129	-44.692	0.98	2.74	J160431-444131	J1604.7-4443	PMN J1604-4441	UNKNOWN	N
242.693	-66.816	0.99	0.93	J161046-664900	J1610.6-6649	CRATES J1610-6649	BLL	Y
242.591	-39.982	0.92	6.52	J161021-395857	J1610.8-3955	VCS2 J1610-3958	FSRQ	N
244.324	-58.801	0.95	5.51	J161717-584806	J1617.7-5843	PMN J1617-5848	UNKNOWN	N
244.455	-77.288	0.99	1.04	J161749-771718	J1617.9-7716	PKS 1610-77	FSRQ	Y
246.445	-25.460	0.98	2.83	J162546-252739	J1625.7-2524	PKS 1622-253	FSRQ	Y
246.525	-29.857	0.95	5.45	J162606-295126	J1626.2-2956	PKS 1622-29	FSRQ	Y
247.227	-61.876	0.93	6.45	J162854-615236	J1629.5-6147	PMN J1628-6152	UNKNOWN	N
252.569	-50.746	0.99	2.78	J165016-504446	J1650.4-5042	PMN J1650-5044	UNKNOWN	N
255.901	-62.210	0.86	7.63	J170336-621238	J1702.7-6217	CGRABS J1703-6212	FSRQ	N
259.400	-33.701	0.93	5.08	J171736-334206	J1717.9-3343	TXS 1714-336	BLL	N
270.677	-39.668	0.98	1.97	J180242-394007	J1802.5-3939	BZU J1802-3940	UNKNOWN	N
278.129	-56.989	0.97	1.34	J183231-565920	J1832.6-5700	CRATES J1832-5659	BLL	Y
278.416	-21.061	0.99	0.60	J183339-210341	J1833.6-2103	PKS 1830-21	FSRQ	N
282.357	-43.236	0.99	1.99	J184925-431412	J1849.6-4314	CRATES J1849-4314	BLL	Y
287.790	-20.115	0.99	1.11	J191109-200655	J1911.2-2007	PKS B1908-201	FSRQ	Y
289.437	-19.358	0.99	0.47	J191744-192131	J1917.7-1922	CGRABS J1917-1921	BLL	Y
289.566	-41.192	0.99	3.96	J191816-411131	J1918.4-4108	CRATES J1918-4111	BLL	Y
290.35	-12.531	0.96	4.86	J192124-123154	J1921.1-1234	CRATES J1921-1231	UNKNOWN	Y
290.884	-21.075	0.99	0.07	J192332-210433	J1923.5-2104	OV -235	FSRQ	Y
291.263	-10.303	0.99	1.14	J192503-101812	J1925.1-1018	CRATES J1925-1018	BLL	Y
294.317	-39.967	0.80	11.4	J193716-395801	J1938.2-3957	PKS 1933-400	FSRQ	N
296.497	-31.193	0.90	7.22	J194559-311138	J1946.1-3118	PKS 1942-313	BLL	Y
298.671	-11.389	0.98	2.55	J195441-112323	J1954.8-1124	CGRABS J1954-1123	FSRQ	Y
299.805	-42.768	0.97	4.39	J195913-424607	J1959.3-4241	CGRABS J1959-4246	FSRQ	Y
300.237	-17.815	0.99	0.90	J200057-174857	J2000.9-1749	PKS 1958-179	FSRQ	Y
301.98	-44.578	0.96	4.38	J200755-443444	J2007.9-4430	PKS 2004-447	AGN ^(d)	Y
302.102	-4.308	0.96	3.51	J200824-041829	J2008.6-0419	3C 407	AGN	Y
302.356	-48.831	0.99	0.80	J200925-484953	J2009.5-4849	PKS 2005-489	BLL	Y
303.619	-0.789	0.99	1.27	J201428-004723	J2014.5-0047	AT20G J2014-0047	BLL	N
303.813	-1.625	0.80	7.99	J201515-013731	J2015.3-0129	PKS 2012-017	BLL	Y
306.419	-7.597	0.99	0.13	J202540-073551	J2025.6-0735	PKS 2023-07	FSRQ	Y
306.473	-28.763	0.86	7.04	J202553-284547	J2025.9-2852	CGRABS J2025-2845	UNKNOWN	Y
314.068	-47.246	0.99	0.84	J205616-471447	J2056.3-4714	PKS 2052-47	FSRQ	Y
315.909	-62.540	0.94	5.46	J210338-623225	J2103.9-6237	CRATES J2103-6232	UNKNOWN	Y
321.627	-46.096	0.95	4.56	J212630-460548	J2126.1-4603	PKS 2123-463	FSRQ	Y

RA deg	Dec deg	P	Sep arcmin	AT20G	1FGL	1LAC	Class	Clean
323.542	-1.887	0.86	10.3	J213410-015316	J2134.0-0203	4C -02.81	FSRQ	Y
323.833	-50.114	0.88	10.8	J213520-500651	J2135.8-4957	CRATES J2135-5006	FSRQ	Y
324.850	-42.588	0.99	0.08	J213924-423520	J2139.3-4235	CRATES J2139-4235	BLL	Y
326.251	-33.954	0.96	5.07	J214501-335716	J2145.4-3358	CGRABS J2145-3357	FSRQ	Y
329.526	-15.019	0.96	3.02	J215806-150109	J2157.9-1503	PKS 2155-152	FSRQ	Y
329.717	-30.225	0.99	0.55	J215852-301332	J2158.8-3013	PKS 2155-304	BLL	Y
331.680	-0.517	0.86	11.6	J220643-003103	J2207.1-0021	CGRABS J2206-0031	BLL	N
331.932	-53.776	0.97	2.55	J220743-534633	J2207.8-5344	PKS 2204-54	FSRQ	Y
333.260	-25.491	0.98	1.35	J221302-252930	J2213.1-2529	PKS 2210-25	FSRQ	Y
336.447	-4.950	0.99	1.55	J222547-045701	J2225.8-0457	3C 446	FSRQ	Y
337.416	-8.548	0.99	1.87	J222940-083254	J2229.7-0832	PKS 2227-08	FSRQ	Y
339.141	-14.556	0.99	1.44	J223634-143322	J2236.4-1432	PKS 2233-148	BLL	Y
339.283	-39.360	0.96	2.50	J223708-392137	J2237.2-3919	CRATES J2237-3921	FSRQ	Y
340.860	-25.742	0.93	5.20	J224326-254431	J2243.1-2541	PKS 2240-260	BLL	Y
342.685	-28.111	0.97	3.56	J225044-280639	J2250.8-2809	CGRABS J2250-2806	AGN	Y
344.171	-20.194	0.97	4.96	J225641-201141	J2256.3-2009	PKS 2254-204	BLL	Y
344.524	-27.972	0.96	1.63	J225805-275821	J2258.0-2757	PKS 2255-282	FSRQ	N
348.935	-50.310	0.92	4.82	J231544-501839	J2315.9-5014	PKS 2312-505	BLL	Y
350.883	-3.284	0.98	1.72	J232331-031705	J2323.5-0315	PKS 2320-035	FSRQ	Y
351.362	-48.004	0.97	2.56	J232526-480017	J2325.6-4758	PKS 2322-482	BLL	Y
352.337	-49.927	0.99	1.67	J232921-495539	J2329.2-4954	PKS 2326-502	FSRQ	Y
352.766	-21.804	0.98	2.97	J233104-214815	J2331.0-2145	CRATES J2331-2148	FSRQ	Y
354.489	-2.515	0.87	6.36	J233757-023057	J2338.3-0231	PKS 2335-027	FSRQ	Y
357.010	-16.519	0.99	1.88	J234802-163111	J2348.0-1629	PKS 2345-16	FSRQ	Y

Table 3: 222 associations found from the cross correlation of the 1FGL sample and the AT20G survey and classified as blazars in the 1LAC sample. The position of the AT20G radio counterpart, the probability of the association, the angular separation between the radio counterpart and the *Fermi* 1FGL centroid are given. The classification of the source in the 1LAC (FSRQ, BLL or UNKNOWN) is given with the name of the counterpart associated in the 1LAC sample. The last column is a flag: Y=the source is classified as a high confidence blazar in the 1LAC sample and it belongs to the “clean” sub-sample (see A10a for details).

(a) NGC 253, starburst galaxy, (Abdo et al., 2010b).

(b) NGC 4945, starburst/Seyfert 2 (Lenc & Tingay, 2009).

(c) PKS 0625-35, Low-Excitation FRI radio galaxy (Gliozzi et al., 2008).

(d) PKS 2004-447, narrow-Line Seyfert 1 (Abdo et al., 2009b).